HHS Public Access

Author manuscript

Nat Neurosci. Author manuscript; available in PMC 2015 June 01.

Published in final edited form as:

Nat Neurosci. 2014 December ; 17(12): 1664–1672. doi:10.1038/nn.3859.

A HIERARCHY OF ANKYRIN/SPECTRIN COMPLEXES CLUSTERS SODIUM CHANNELS AT NODES OF RANVIER

Tammy Szu-Yu Ho[1], **Daniel R. Zollinger**[2], **Kae-Jiun Chang**[1], **Mingxuan Xu**[3], **Edward C. Cooper**[2,3], **Michael C. Stankewich**[4], **Vann Bennett**[5], and **Matthew N. Rasband**[1,2,*]

[1]Program in Developmental Biology, Baylor College of Medicine, Houston, TX 77030

[2]Department of Neuroscience, Baylor College of Medicine, Houston, TX 77030

[3]Department of Neurology, Baylor College of Medicine, Houston, TX 77030

[4]Department of Pathology, Yale University, New Haven, CT 06520

[5]Department of Cell Biology, Duke University, Durham, NC 27710

SUMMARY

The scaffolding protein ankyrinG is required for Na+ channel clustering at axon initial segments. It is also considered essential for Na+ channel clustering at nodes of Ranvier to facilitate fast and efficient action potential propagation. However, in contrast to these widely accepted roles, we show here that ankyrinG is dispensable for nodal Na+ channel clustering *in vivo*. Surprisingly, without ankyrinG, erythrocyte ankyrin (ankyrinR) and its binding partner βI spectrin substitute and rescue nodal Na+ channel clustering. In addition, channel clustering is also rescued after loss of nodal βIV spectrin by βI spectrin and ankyrinR. In mice lacking both ankyrinG and ankyrinR, Na+ channels fail to cluster at nodes. Thus, ankyrinR/βI spectrin protein complexes function as secondary reserve Na+ channel clustering machinery, and two independent ankyrin/spectrin protein complexes exist in myelinated axons to cluster Na+ channels at nodes of Ranvier.

The high density of Na+ channels at nodes of Ranvier is an essential feature of myelinated axons and facilitated the evolution of the complex and efficient vertebrate nervous system [1]. Nodal Na+ channel clusters confer several important advantages including decreased energy and space requirements, and increased action potential conduction velocity.

*Correspondence should be addressed to: Dr. Matthew N. Rasband, Department of Neuroscience, Baylor College of Medicine, One Baylor Plaza, Houston, Texas 77030, Tel: 713-798-4494, Fax: 713-798-3946, rasband@bcm.edu.

Competing Financial Interests:
The authors declare no competing financial interests.

Supplemental Information
Supplemental Information includes nine figures and can be found with this article online.

AUTHOR CONTRIBUTIONS

M.N.R. and T. S. H. conceived the project, designed the experiments and wrote the manuscript. D.R.Z. performed the electrophysiology experiments and analyzed the data. T.S.H. performed all other experiments and analyzed the data. K.-J.C. supervised the RT-qPCR experiments. K.-J.C., M.X., E.C.C., M.C.S. and V.B. provided crucial reagents, mice and support.

Three overlapping mechanisms work together to cluster Na+ channels at nodes. These include 1) aglia-derived extracellular matrix (ECM) that interacts with and clusters the axonal cell adhesion molecule neurofascin-186 (NF186), 2) paranodal axoglial junctions that restrict the location of nodal proteins between adjacent myelin segments, and 3) submembranous cytoskeletal proteins (βIV spectrin) that link the nodal Na+ channel protein complex to the actin-based axonal cytoskeleton [2–5]. These three mechanisms of channel clustering converge on the scaffolding protein ankyrinG (AnkG) [6]. AnkG is highly enriched at nodes of Ranvier where it interacts directly and simultaneously with Na+ channels, NF186, and βIV spectrin; the AnkG-binding domains of these proteins are necessary and sufficient for their nodal localization [7–10]. Reduction in AnkG expression by shRNA in myelinated dorsal root ganglion-Schwann cell co-cultures was reported to block the clustering of Na+ channels at nodes [10]. Similarly, loss of AnkG from axon initial segments (AIS) blocks the clustering of these same proteins at the AIS [11–13].

Together, these observations have led to the widely accepted model that neuron-glia interactions first gather NF186 in the axonal membrane. Next, clustered NF186 functions as a nucleation site for nascent node assembly by recruiting and clustering AnkG. Na+ channels are enriched at nodes through their AnkG-binding motif [9, 14, 15]. Finally, the entire NF186-AnkG-Na+ channel protein complex is stabilized and linked to the actin cytoskeleton through βIV spectrin. Further support for this sequence of events has come from the analysis of mutant mice lacking paranodal neuron-glia interactions, nodal NF186-binding ECM proteins, NF186, or βIV spectrin [2, 4, 5, 16]. Thus, AnkG's requirement for nodal Na+ channel clustering at nodes of Ranvier *in vivo* is broadly accepted [17–20].

Here, using AnkG conditional knockout mice, we show that in contrast to the widely accepted model, AnkG is dispensable for Na+ channel clustering at nodes of Ranvier. Remarkably, we found a second, non-dominant ankyrinR (AnkR)/βI spectrin protein complex (traditionally thought to function mainly in erythrocytes) that is also found in myelinated axons and that can function as a reserve mechanism to rescue Na+ channel clustering. We show that the interactions between NF186, Na+ channels, and the two distinct ankyrin/spectrin complexes have different affinities leading to a hierarchy of clustering activities. Finally, by generating mice deficient in both AnkG and AnkR, we prove that ankyrins are required for nodal Na+ channel clustering.

RESULTS

AnkG conditional knockout mice

To investigate the requirement for AnkG to cluster Na+ channels at nodes of Ranvier *in vivo*, we generated a conditional null mutant allele where exons 23 and 24 of the AnkG gene (*Ank3*) are flanked by LoxP sites (*Ank3*$^{F/F}$ mice) and can be excised in the presence of Cre recombinase. To confirm the utility of these mice and loss of AnkG expression, we first used *Nestin-Cre* mice to eliminate neuronal AnkG. *Nestin-Cre;Ank3*$^{F/F}$ mice died at birth and failed to form AISs. Immunostaining of developing cortex at postnatal day 0 (P0) in control mice revealed widespread AIS βIV spectrin and AnkG throughout the cortical plate (Figs. 1a, b; AnkG staining not shown). In contrast, *Nestin-Cre;Ank3*$^{F/F}$ mice lacked AISs (Fig. 1c). Na+ channels were clustered at the AIS of individual cortical neurons in control mice

where they colocalized with AnkG (Fig. 1d, e, arrows, and Supplementary Fig. 1a), but *Nestin-Cre;Ank3*$^{F/F}$ mice lacked Na+ channel clustering in the cortex except in those few neurons that did not undergo recombination (Fig. 1f, arrow). Immunoblots confirmed the nearly complete loss of AnkG protein from brains of *Nestin-Cre;Ank3*$^{F/F}$ mice (Fig. 1j). Together, these results showed that AnkG is required for AIS assembly *in vivo*, and that *Ank3*$^{F/F}$ mice can be used to study the function of AnkG *in vivo*.

AnkG is dispensable for nodal Na+ channel clustering

Since *Nestin-Cre;Ank3*$^{F/F}$ mice die at birth, and myelination is a postnatal event, they cannot be used to study node of Ranvier formation. Therefore, to circumvent the perinatal lethality, we used *Advilin*$^{Cre/+}$ (*Avil-Cre*) and *Six3-Cre* mice to specifically eliminate AnkG expression in peripheral sensory neurons and retinal ganglion cells, respectively [21, 22]. We reasoned that more restricted recombination might allow mice to survive past birth and permit the analysis of node assembly in the absence of AnkG. *Avil-Cre;Ank3*$^{F/F}$ mice are also useful since recombination only occurs in sensory neurons, allowing for a direct comparision between dorsal (sensory) and ventral (motor) roots from the same animal. *Avil-Cre;Ank3*$^{F/F}$ and *Six3-Cre;Ank3*$^{F/F}$ mice appeared normal at birth.

To confirm loss of AnkG from nodes of Ranvier and to determine if AnkG is required for nodal Na+ channel clustering, we immunostained P14 dorsal roots from *Ank3*$^{F/F}$ and *Avil-Cre;Ank3*$^{F/F}$ mice, and ventral roots (control) from *Avil-Cre;Ank3*$^{F/F}$ mice. Whereas control roots had intense AnkG and Na+ channel immunoreactivity at nodes (Fig. 1g, h, arrows), *Avil-Cre;Ank3*$^{F/F}$ dorsal roots were completely devoid of nodal AnkG (Fig. 1i, k). Surprisingly, we found normal enrichment of Na+ channels at nodes in AnkG-deficient dorsal roots (Fig. 1i, arrows, k).

To determine if *Avil-Cre;Ank3*$^{F/F}$ sensory roots were functionally impaired, we measured their conduction velocity at P14. We found no difference between control and AnkG-deficient roots (4.14±0.31 m s^{-1} in control and 4.02±0.39 m s^{-1} in AnkG-deficient roots. N= 11 dorsal roots from 3 mice per genotype. p=0.79, unpaired two-tailed t-test). We also observed no difference in compound action potential waveform (Supplementary Fig. 1d). Similarly, at P28 *Avil-Cre;Ank3*$^{F/F}$ mice showed no impairment on the rotarod (latency to fall from the rotarod: 163.2±10.7 s and 151.7±15.5 s for *Ank3*$^{F/F}$ and *Avil-Cre; Ank3*$^{F/F}$ mice, respectively. N= 8 mice of each genotype. p=0.55, unpaired two-tailed t-test), the wire hang test (Supplementary Fig. 1b), or thermal nociception (Supplementary Fig. 1c). Similar to *Avil-Cre;Ank3*$^{F/F}$ mice, we found Na+ channel clustering in the optic nerves of *Six3-Cre;Ank3*$^{F/F}$ mice in the absence of AnkG (Fig. 1l). *Avil-Cre;Ank3*$^{F/F}$ and *Six3-Cre;Ank3*$^{F/F}$ mice were fertile and appeared normal with no signs of impairment or loss of Na+ channel clustering even at two years and 18 months of age, respectively (Supplementary Fig. 2a, b, and Supplementary movies 1–4). Thus, AnkG is dispensable for Na+ channel clustering and axon function in both the peripheral and central nervous systems.

Although we found no difference in Na+ channel clustering between control and AnkG-deficient roots at P14, when we examined node formation during early development, we found a significantly reduced density of Na+ channels in *Avil-Cre;Ank3*$^{F/F}$ dorsal roots

(Supplementary Figs. 1e, f). Thus, although AnkG is dispensable for Na+ channel clustering, the compensatory mechanism that rescues channel clustering is less efficient.

AnkR rescues Na+ channel clustering

We previously showed the AnkG-binding motif in Na+ channels is both necessary and sufficient for its localization to nodes of Ranvier [9]. If the results of that study are correct, how can Na+ channels be clustered at nodes without AnkG? While it is possible that some ankyrin-independent mechanism can also facilitate Na+ channel clustering through this motif, a simpler explanation is that channel clustering is rescued through compensation by another ankyrin that can also interact with Na+ channels at the AnkG-binding motif. Vertebrates have 3 ankyrins: AnkG (*Ank3*), AnkB (*Ank2*), and AnkR (*Ank1*). AnkB has previously been reported to be localized in unmyelinated axons [23–25] and at paranodes of myelinated axons [26]. Furthermore, AnkB-deficient mice die shortly after birth due, in part, to widespread nervous system defects [27]. AnkR, also known as erythrocyte ankyrin, functions in red blood cells to link the Cl^-/HCO_3^- anion exchanger to the submembranous spectrin cytoskeleton [28]. Mutations in AnkR cause hereditary spherocytosis [29].

To determine if Na+ channel clustering is rescued in *Avil-Cre;Ank3*$^{F/F}$ sensory neurons by AnkB or AnkR, we performed triple immunostaining for AnkG, AnkB, and AnkR. Consistent with previous reports, control dorsal roots had nodal AnkG (blue) and paranodal AnkB (red), but little or no nodal AnkR immunoreactivity (Fig. 2a, arrows). Remarkably, in AnkG-deficient dorsal roots we found a dramatic increase in AnkR immunoreactivity (green) at nodes (Fig. 2b, arrows), but no change in AnkB (red). When we immunostained control optic nerve axons using antibodies against AnkG and AnkR we found robust AnkG immunoreactivity at nodes and paranodes but no nodal AnkR (Fig. 2c, arrow [30]; paranodal AnkG is oligodendroglial in origin; KJ Chang and MN Rasband, unpublished results). However, when we examined *Six3-Cre;Ank3*$^{F/F}$ optic nerve axons we found that nodes deficient in AnkG had robust AnkR immunoreactivity (Fig. 2d, arrows). Thus, AnkR is found at nodes in AnkG-deficient axons and may substitute for AnkG.

AnkR colocalizes with Na+ channels at nodes of Ranvier in AnkG-deficient neurons (Supplementary Fig. 3a, b). To confirm that AnkR can substitute for AnkG and interact with Na+ channels, we generated GST fusion proteins containing the intracellular loop 2 AnkG-binding motif (GST-Nav II–III) and performed pull-down experiments with AnkG and AnkR; phosphorylation of several key serine residues in GST-Nav II–III by the kinase CK2 significantly enhances its binding affinity for ankyrins [31]. We found that although both AnkG and AnkR can interact with Na+ channels, it was necessary to dramatically increase the amount of AnkR input to begin to detect an interaction (Fig. 2e), suggesting AnkG's preference for binding GST-Nav II–III is much higher than that of AnkR.

The remarkable rescue of Na+ channel clustering by AnkR during development led us to ask if AnkR could also preserve Na+ channel clustering after loss of AnkG in adult neurons. To test this possibility, we injected AAV-GFP or AAV-CreGFP into the eyes of P21 *Ank3*$^{F/F}$ mice to transduce retinal ganglion cells (RGCs). 2-months later, the axons of transduced RGCs were easily identified by GFP immunoreactivity (Fig. 3). The axons of RGCs transduced with AAV-GFP had normal AnkG (Fig. 3a, g), normal Na+ channel clustering

(Fig. 3c, g), and no nodal AnkR immunoreactivity (Fig. 3e, g). We also found that although 86% of nodes along the axons of RGCs transduced with AAV-CreGFP had no AnkG (Fig. 3b, arrows, g), 93% had Na+ channel clustering (Fig. 3d, arrows, g). Consistent with the preservation of many nodal Na+ channel clusters, we found 75% of nodes along GFP-labeled axons had AnkR immunoreactivity (Fig. 3f, arrows, g). Thus, AnkR also compensates for loss of AnkG in mature, fully myelinated axons and can rescue Na+ channel clustering.

βI spectrin replaces βIV spectrin in AnkG-deficient axons

βIV spectrin is also clustered at nodes of Ranvier (Supplementary Fig. 4a) where it links Na + channels and AnkG to the submembranous cytoskeleton. Intriguingly, loss of nodal AnkG is accompanied by a dramatic reduction of βIV spectrin and even a complete loss of βIV spectrin at some nodes (Supplementary Fig. 4b, arrow). Without βIV spectrin how can nodes be maintained? We wondered if some β spectrin other than βIV might preferentially partner with AnkR to rescue Na+ channel clustering and stabilization at nodes. In erythrocytes, AnkR's spectrin binding partner is βI spectrin [7]. Therefore, to determine if βI spectrin also contributes to the rescue of nodes in AnkG-deficient axons, we immunostained control and *Avil-Cre;Ank3*$^{F/F}$ mice using antibodies against βI spectrin. In control dorsal roots the vast majority of nodes had βIV spectrin and were devoid of any βI spectrin (Fig. 4a, inset and arrowheads, c). In contrast, *Avil-Cre;Ank3*$^{F/F}$ dorsal roots frequently had robust nodal βI spectrin staining (Fig. 4b, arrows, c); both *Avil-Cre;Ank3*$^{F/F}$ dorsal roots and *Six3-Cre;Ank3*$^{F/F}$ optic nerves had βI spectrin that colocalized with Na+ channels (Supplementary Fig. 3c, d). Furthermore, there was often a mutually exclusive relationship between βIV spectrin and βI spectrin at nodes: nodes with βIV spectrin had no βI spectrin (Fig. 4b, arrowheads), and nodes with βI spectrin had no βIV spectrin (Fig. 4b, arrows). Thus, Na+ channel clustering in AnkG-deficient axons is rescued not only by substitution of a single protein, but instead the entire AnkG-βIV spectrin protein complex is replaced by AnkR-βI spectrin.

To determine if AnkG and AnkR favor binding of one spectrin over another, we co-expressed GFP-tagged AnkG or AnkR together with a fragment of βI spectrin or βIV spectrin containing the ankyrin-binding spectrin repeat [8]. We found that βI spectrin's binding activity was much higher for AnkR than for AnkG (Fig. 4d, e), and that βIV spectrin preferentially interacts with AnkG rather than AnkR (Fig. 4e, f).

AnkR and βI spectrin rescue βIV spectrin-deficient axons

Since AnkR and βI spectrin substitute for AnkG and βIV spectrin in AnkG-deficient axons, we reasoned that a similar substitution should occur in βIV spectrin-deficient axons. To test this possibility, we used 'quivering 3J' mutant mice (*Spnb4*$^{qv3J/qv3J}$) which have a frame shift mutation resulting in truncated βIV spectrin [32] and loss of βIV spectrin from nodes [2]. Although *Spnb4*$^{qv3J/qv3J}$ mice have progressive ataxia and widened nodes of Ranvier, they still cluster Na+ channels at nodes [33]. Neither βI spectrin nor AnkR were detected at control optic nerve nodes of Ranvier (Fig. 5a, c, arrows, e). Remarkably, immunostaining of optic nerves from *Spnb4*$^{qv3J/qv3J}$ mice showed robust nodal βI spectrin at every node (Fig. 5b, arrows, e), and AnkR immunoreactivity at 68% of nodes (Fig. 5d, arrows, e). These results

demonstrated that AnkG and βIV spectrin form the primary ankyrin-spectrin complex at nodes and suggest that loss or disruption of either AnkG or βIV spectrin permits a secondary ankyrin-spectrin complex consisting of AnkR and βI spectrin to rescue Na+ channel clustering.

Nodal AnkR and βI spectrin derive from pre-existing pools

What is the source of the AnkR and βI spectrin that rescues nodal Na+ channel clustering in AnkG- and βIV spectrin-deficient axons? We considered two possibilities: the nodal AnkR and βI spectrin could 1) be newly synthesized in response to loss of AnkG or βIV spectrin, or 2) comprise a pre-existing pool of unclustered protein complexes not detectable by immunostaining. To distinguish between the two, we performed reverse transcription-quantitative polymerase chain reaction (RT-qPCR) and measured the relative AnkG, AnkR, βIV spectrin, and βI spectrin transcript levels in *Ank3*$^{F/F}$ and *Avil-Cre;Ank3*$^{F/F}$ DRG neurons. Although AnkG transcripts were nearly undetectable in *Avil-Cre;Ank3*$^{F/F}$ mice, we observed no change in the expression levels of AnkR, βIV spectrin, or βI spectrin in response to loss of AnkG (Fig. 6a), suggesting that transciptional upregulation does not account for the nodal substitution by AnkR and βI spectrin.

Consistent with the idea that AnkR and βI spectrin comprise a pre-existing pool of axonal proteins, we found that compared to controls, their protein levels in postnatal day 0.5 AnkG-deficient brain (*Nestin-Cre;Ank3*$^{F/F}$; Fig. 6b) and postnatal days 14, 31, and 4 month-old dorsal root homogenates (*Avil-Cre;Ank3*$^{F/F}$; Fig. 6c **and** Supplementary Fig. 5a) remain unchanged. If AnkR-βI spectrin complexes are normally found in the axon and can be clustered at nodes when AnkG is not present, we reasoned that a nascent node, consisting primarily of clustered NF186, might provide a substrate for both AnkG and AnkR binding during early development, resulting in nodes labeled for both AnkG and AnkR. To test this possibility, we immunostained developing sciatic nerve and optic nerve with antibodies against AnkG and AnkR. We found that in sciatic nerve AnkR could be detected at nearly every node of Ranvier during the first two weeks of development (Fig. 6f, arrows, d). However, the nodal AnkR was transient and rapidly decreased in both intensity and frequency of nodal staining, such that by P30, 40% of nodes had no detectable AnkR, and the remaining nodes had very little AnkR that was only weakly detected by immunostaining(Fig. 6d). Furthermore, the AnkR fluorescence intensity observed in wild-type animals was always much less than the AnkR fluorescence intensity observed in *Avil-Cre;Ank3*$^{F/F}$ mice (Fig. 6d). In contrast to the PNS, AnkR was detected at very few forming nodes of Ranvier in the CNS (Supplementary Fig. 5b). This may reflect differences in the primary mechanisms of node assembly between the PNS and CNS [2].

Why does AnkR gradually disappear from PNS nodes with increasing age? The simplest explanation is that AnkG's affinity for NF186 may be higher than AnkR's affinity for NF186. To test this possibility we performed co-immunoprecipitation experiments using epitope-tagged NF186, NF186 lacking its ankyrin-binding motif (NF186Δ FIGQY), and membrane binding domains (MBD) of AnkR and AnkG. We found that AnkG's binding activity for NF186 was much higher than AnkR's (Fig. 6e). Taken together, these results support the conclusion that a pre-existing pool of AnkR and βI spectrin are found in axons

and upon loss of AnkG or βIV spectrin these proteins redistribute to nodes to rescue Na+ channel clustering.

AnkR is not required for nodal Na+ channel clustering

Since AnkR is found at nodes during early development (Fig. 6f), we sought to determine if it contributes to normal node formation. To test this possibility, we obtained AnkR-deficient mice (*Ank1*$^{pale/pale}$). The *Ank1*$^{pale/pale}$ mice have severe hemolytic anemia, a pale appearance, and usually die before P7. In rare instances *Ank1*$^{pale/pale}$ mice can survive for several weeks. Both immunoblot analysis of brain homogenates (Fig. 7a) and immunostaining of P5 sciatic nerve or P22 optic nerve showed no detectable AnkR (Fig. 7c, d). Nodes of Ranvier formed normally in the PNS and CNS of *Ank1*$^{pale/pale}$ mice, and were highly enriched in Na+ channels (Fig. 7b–d). Thus, AnkR is not essential for normal node of Ranvier assembly.

Ankyrins are required for nodal Na+ channel clustering

Although both AnkG and AnkR are by themselves dispensable for Na+ channel clustering at nodes of Ranvier, previous studies indicated the AnkG-binding motif in the II–III linker domain of Na+ channels is both necessary and sufficient for nodal channel clustering [9]. To finally prove that ankyrins are required for nodal Na+ channel clustering, we generated mice deficient for both AnkG and AnkR. *Avil-Cre;Ank3*$^{F/F}$*; Ank1*$^{pale/pale}$ mice lack AnkG and AnkR in DRG sensory neurons. These mice usually died at or before P3, although we obtained a few animals that survived from P4–P7. At P3 both *Ank3*$^{F/F}$ and *Avil-Cre;Ank3*$^{F/F}$ mice had Na+ channel clustering at nodes. In stark contrast, *Avil-Cre;Ank3*$^{F/F}$*; Ank1*$^{pale/pale}$ mice had no detectable Na+ channels between neurofascin (NF) -labeled paranodes (Fig. 8a, b). Similarly, in animals that survived from P4–P7, although we found many Caspr-labeled paranodes, some of which had well-defined gaps between them indicating a node (Fig. 8d, arrow), we were unable to detect any Na+ channel clusters between or flanking these Caspr-labeled paranodal junctions. Quantification of the percentage of nodes with Na+ channel clusters showed that animals lacking both AnkG and AnkR had virtually no detectable Na+ channel clusters in their dorsal roots (Fig. 8b). Thus, axonal ankyrins are required for Na+ channel clustering at nodes of Ranvier.

DISCUSSION

Nodes of Ranvier are a remarkable example of reciprocal subcellular differentiation. Their evolution has been proposed as a key adaption in the divergence and success of vertebrates [1]. Loss or disruption of nodes by disease, autoimmune attack, or injury can cause nervous system dysfunction and even death [34]. Thus, elucidating how nodes are assembled is essential to understand nervous system function, and is an important consideration for any therapeutic strategy aimed at nervous system repair or regeneration.

A new nodal ankyrin/spectrin protein complex

Neurons and myelinating glia interact to facilitate the high density clustering of voltage-gated Na+ channels. Many of the protein-protein interactions contributing to node formation have been described, and the model placing AnkG at the nexus of nodal Na+ channel

clustering is widely accepted [35]. Here, we tested this model in both the PNS and CNS by generating mice with AnkG-deficient dorsal root ganglia and retinal ganglion cells, respectively. Much to our surprise and in stark contrast to its reported necessity [10, 36], we found that AnkG is dispensable for nodal Na+ channel clustering. Remarkably, we discovered another clustering mechanism that depends on a second ankyrin/spectrin protein complex consisting of AnkR and βI spectrin, both of which were previously thought of as 'erythrocyte' in nature [37]. Furthermore, loss of βIV spectrin also led to replacement of AnkG by AnkR/βI spectrin and preservation of Na+ channel clustering (Supplementary Fig. 6a). The rescue of Na+ channel clustering and nervous system function in AnkG-deficient neurons by AnkR is a striking example of compensation. The rescue of Na+ channel clustering is even more remarkable since compensation occurs not by just a single protein, but by a protein complex.

In support of an AnkG-independent clustering mechanism, Zhang et al. [38] investigated the sources and targeting of proteins to nodes of Ranvier. They induced myelination of degeneration resistant axons separated from neuronal cell bodies and observed a small minority of Na+ channel clusters (~20%) at newly formed heminodes that had only weak or undetectable AnkG staining. We suggest that this small population of Na+ channel clusters may have accumulated through the actions of AnkR.

Our results are likely generalizable to all myelinated axons rather than a tissue or cell-type specific phenomenon since DRG and RGC neurons have different embryonic origins (neural crest and neuroectoderm, respectively). However, Barry et al. [36] recently reported that AnkG is required for axonal trafficking and nodal clustering of Na+ channels based on their examination of a constitutive knockout mouse lacking exon 1b of AnkG (ex1b AnkG KO; AnkG has five identified alternative first exons); exon 1b-containing AnkG was previously thought to be mainly expressed in cerebellum and Purkinje neurons [11]. We also analyzed ex1b AnkG KO mice, but in contrast to their results, we found robust nodal Na+ channel clustering at AnkG-deficient nodes (Supplementary Fig. 7). Despite loss of AnkG from PNS and CNS axons, we found Na+ channels clustered at nodes, indicating AnkG is required neither for nodal clustering nor for axonal trafficking of Na+ channels. We are unable to explain the discrepancy between their results and ours, although the complexity of AnkG's alternative splicing and the expression of exon 1b-containing AnkG in both Purkinje neurons and oligodendrocytes [39] favors the more specific experimental approach used in our study. Nevertheless, since AnkR binds Na+ channels and is found in axons, the axonal trafficking of Na+ channels may still depend on their interaction with ankyrins.

A hierarchy of ankyrin/spectrin interactions

The rescue of Na+ channel clustering by AnkR/βI spectrin is not a consequence of genetic reprogramming, but rather redistribution of a pre-existing pool of axonal AnkR/βI spectrin. If AnkR/βI spectrin complexes are normally found in mature myelinated axons, why are they not at nodes? Our results indicate that AnkR, AnkG, βI spectrin, and βIV spectrin each have different affinities for one another and can interact with Na+ channels and NF186; AnkG has the highest affinity for NF186, Na+ channels, and βIV spectrin, while AnkR has a higher affinity for βI spectrin. This hierarchy of ankyrin/spectrin interactions and preference

for specific binding partners immediately suggests a simple model that can explain the steady state molecular composition of nodes, the transient detection of AnkR/βI spectrin at nodes during early development, and the rescue of Na+ channel clustering in AnkG- or βIV spectrin-deficient axons (Supplementary Fig. 6b). We propose that during early development neuron-glia interactions first cluster NF186, resulting in a local excess of NF186 relative to AnkG and AnkR, allowing both to bind to NF186. Na+ channels are then recruited to developing nodes by binding to either AnkG or AnkR. Over time, turnover of AnkR and the higher affinity of AnkG for NF186 and Na+ channels results in the displacement and gradual loss of AnkR from nodes. The interaction between AnkG and βIV spectrin further stabilizes the NF186-AnkG-Na+ channel complex, resulting in a mature node that includes AnkG and βIV spectrin rather than AnkR and βI spectrin. Although we transiently detected AnkR at developing PNS nodes, we only rarely detected AnkR at developing CNS nodes. This discrepancy may reflect differences between the PNS and CNS in the mechanisms responsible for the initial clustering of NF186 [2, 4] or differences in the temporal expression of ankyrins between the PNS and CNS.

In AnkG-deficient axons, AnkR does not have to compete with AnkG for NF186 or Na+ channels, despite AnkR's decreased binding efficiency compared to AnkG. We speculate the reduced density of Na+ channels seen in AnkG-deficient sensory axons during early development reflects this reduced binding efficiency (Supplementary Fig. 1e, f). Finally, in AnkG-deficient axons the NF186-AnkR-Na+ channel complex is stabilized in the membrane by AnkR's preferential binding to βI spectrin. In βIV spectrin-deficient axons, although AnkG is expressed, we propose that spectrin-actin interactions stabilize the NF186-ankyrin-Na+ channel complex; without βIV spectrin, the balance of stable complexes is shifted towards NF186-AnkR-Na+ channels.

If AnkR/βI spectrin can compensate for loss of AnkG/βIV spectrin, why are AISs not rescued in the *Nestin-Cre;Ank3*$^{F/F}$ mice? Ankyrins are enriched at nodes of Ranvier by interacting with NF186. Thus, nodal clustering of ankyrins depends on extrinsic interactions between NF186 and myelinating glia. In contrast, AIS clustering of AnkG does not depend on any extrinsic factors, but instead AnkG is restricted to the proximal axon by an intra-axonal cytoskeletal boundary consisting of ankyrinB, αII spectrin, and βII spectrin [25]. Interestingly, AnkR is not subject to this intra-axonal cytoskeletal boundary and instead is diffusely distributed throughout neurons (TS Ho and MN Rasband, unpublished results). Immunostaining of dorsal root and retinal ganglion cells in *Avil-Cre;Ank3*$^{F/F}$ and *Six3-Cre;Ank3*$^{F/F}$ mice, respectively, shows no enrichment for Na+ channels or AnkR in an AIS like structure (Supplementary Fig. 8). Future studies comparing AnkG and AnkR may reveal key domains and/or interactions that are necessary for AIS clustering [40].

What is the AnkR/βI spectrin protein complex doing in myelinated axons and the nervous system? Although previous studies have reported AnkR in the brain [41, 42], little is known about its function. AnkR is not required for normal node formation since *Ank1*$^{Pale/Pale}$ mice showed no defect in PNS or CNS node formation (Fig. 7c, d). Another AnkR mutant mouse with normoblastosis (nb/nb mice) and hemolytic anemia also shows reduced levels of AnkR, but can survive for many months. Interestingly, nb/nb mice have cerebellar Purkinje cell degeneration [43], suggesting AnkR may play important roles in the nervous system besides

the node of Ranvier. Furthermore, a few case reports describe patients with hereditary spherocytosis that also show neurological symptoms including spastic paraplegia and cerebellar dysfunction [44].

Ankyrins are required for nodal Na+ channel clustering

AnkG was first reported at nodes and suggested to be responsible for Na+ channel clustering nearly two decades ago [6]. Proof that ankyrins are required for nodal Na+ channel clustering has not been forthcoming due to the lack of appropriate animal models and reagents. Using full-length wild-type and mutant Na+ channel expression constructs, and the ankyrin-binding fragment of Na+ channels, we showed the AnkG-binding motif of Na+ channels is both necessary and sufficient for its localization to nodes [9]. However, the results presented here show that AnkG is dispensable. Instead, the rescue of channel clustering by AnkR in AnkG-deficient neurons indicates the motif in the Na+ channel is more correctly described as an ankyrin-binding motif.

In conclusion, we provide here evidence that a hierarchy of ankyrin/spectrin interactions exists in myelinated axons to cluster nodal Na+ channels. Finally, the analysis of mice deficient for both AnkG and AnkR in dorsal sensory neurons proves that ankyrins are required for Na+ channel clustering at nodes of Ranvier.

METHODS

Animals

AnkG conditional knockout mice were generated by cell-type-specific Cre-mediated deletion of the *Ank3* gene. The targeting construct was designed and $Ank3^{F/F}$ mice were generated as previously described [45]. Exon 1b AnkG KO mice have been described [11]. AnkR mutant mice ($Ank1^{pale/pale}$; C57BL/6) and Nestin-Cre transgenic mice (C57BL/6) were obtained from the Jackson Laboratory (#009157 and #003771, respectively). Advillin-Cre (Avil-Cre) mice were provided by Dr. Fan Wang (Duke University, Durham, NC). Six3-Cre mice were provided by Dr. William H. Klein (University of Texas MD Anderson Cancer Center, Houston, TX). *Avil-Cre;*$Ank3^{F/F}$*;*$Ank1^{pale/pale}$ were generated by crossing *Avil-Cre;*$Ank3^{F/+}$*;*$Ank1^{pale/+}$ with $Ank3^{F/F}$*;*$Ank1^{pale/+}$ mice. βIV spectrin mutant mice ($Spnb4^{qv3j}$)were described previously [32]. Both male and female mice were used in our studies. All mouse work and procedures were approved by the Animal Care and Use Committee at Baylor College of Medicine and were performed in accordance with the NIH guide for the humane care and use of animals.

Antibodies

Mouse monoclonal pan Na^+ channel (pan-Nav) antibody was described previously [30]. Other mouse monoclonal antibodies: AnkG (N106/36, UC Davis/NIH NeuroMab facility), AnkB (N105/17 and N105/13, UC Davis/NIH NeuroMab facility), Caspr (K65/35, UC Davis/NIH NeuroMab facility), GST (N100/13, UC Davis/NIH NeuroMab facility), GFP (N86/38, UC Davis/NIH NeuroMab facility), actin (C4, EMD Millipore), Myc (9E10, Sigma), and HA (16B12, Covance) were used. Rabbit polyclonal antibodies against GFP and neurofilament M were purchased from Life Technologies (cat no. A11122) and EMD Millipore (cat no.

AB1987), respectively. Rabbit antibodies against AnkG were generated against the N-terminal domain. Rabbit anti-AnkR antibodies were made by immunizing rabbits with His-tagged full-length human AnkR protein, followed by affinity purification from rabbit serum. Rabbit anti-β1 spectrin was raised against and affinity purified against the unique C-terminus of βIΣ2 spectrin [46]. Rabbit anti-βIV spectrin antibodies were previously described [47] and chicken anti-βIV spectrin was generated using the same peptide; both antibodies were purified by affinity chromatography against the immunizing peptide. The chicken antibody to neurofascin was purchased from R&D Systems (cat no. AF3235). The goat anti-AnkG antibody was generated against AnkG's C-terminal domain. The rat anti-GFP antibody was purchased from Nacalai USA (Cat. No.: 04404-84). Secondary antibodies were purchased from Jackson ImmunoResearch Laboratories and Life Technologies.

DNA constructs

The full-length rat 270-kDa AnkG-GFP has been described [40]. To construct Myc-tagged AnkG membrane binding domain (Myc-AnkG MBD), the DNA fragment encoding 1–846 amino acids (aa) of AnkG was PCR amplified and inserted into the EcoRI-XbaI sites of pCS3+MT vector (a gift from Dr. Dave Turner, University of Michigan, Ann Arbor, MI). The primers for amplifying AnkG MBD are forward, TCCGAATTCAATGGCTCATGCCGCCTCCCAG, and reverse, GCTCTAGAGTTTCTGGGACATTCATTTTGTG. The Flag-tagged full-length human AnkR (Flag-AnkR) was generated from the *Ank1* isoform 1(NM_020476.2 CDS). The GFP-tagged full-length human AnkR was made by introducing EGFP into the KpnI-EcoRV sites of Flag-AnkR while keeping in-frame with the upstream Flag tag and the downstream AnkR protein. Myc-tagged AnkR membrane binding domain (Myc-AnkR MBD) was made by PCR (1–827aa of AnkR, NP_065209.2) and cloned into pCS3+MT vector through the EcoRI-XhoI sites. The primers for amplifying AnkR MBD are forward, TCCGAATTCAATGCCCTATTCTGTGG and reverse, GCCTCGAGGAAGCTGATGAGTTCTTCC. HA-tagged full-length neurofascin 186-kDa isoform (pEGFP-N1-HA-NF186) was a gift from Dr. Stephen Lambert (University of Central Florida). pEGFP-N1-HA-NF186Δ FIGQY was constructed by PCR amplification of two fragments flanking TTTATTGGCCAGTAC (encoding FIGQY) with forward, AAATGGGCGGTAGGCGTG + reverse, GGAGCCATCTTCGTTGAAC and forward, ACTGTCAGAAAGGACAAGG + reverse, GAACTTGTGGCCGTTTAC, and replacing the insert between XhoI and SpeI sites of pEGFP-N1-HA-NF186 with the two PCR fragments digested with XhoI and SpeI, respectively. Myc-tagged spectrin repeat 10–15 (SR10–15) of βIV spectrin was described previously [8]. To construct Myc-tagged βI spectrin ankyrin-binding domain, the DNA fragment encoding SR13–17 of βI spectrin was PCR amplified from the construct GST-βI spectrin SR13–17 (a gift from Dr. Shane Cunha, University of Texas Health Sciences Center) and introduced into the EcoRI-XbaI sites of pCS3+MT vector. The primers for amplifying SR13–17 are forward, TCCGAATTCACTCTATGTCATCTCCG, and reverse GCTCTAGAGGCAGTGACTCCCAGGAAC. GST-Nav II–III was generated by PCR amplification using the rat Nav1.2 cDNA clone [48] as template, and primers: GAAGGATCCGACAACCTGGCTGCCACAGATGACG (forward) and GAAGTCGACTCACTTGTAGCACGTTTTCCTCAAGTTCC (reverse). The PCR product,

corresponding to residues 989–1203, representing the entire domain II–III intracellular loop, was inserted into BamHI+SalI sites of pGEX4T-1.

Immunofluorescence and Image Analysis

Nervous system tissues were dissected and fixed in 4% paraformaldehyde for 30 min (optic nerves, sciatic nerves and nerve roots) to 1 hour (brains) on ice and subsequently immersed in 20% sucrose overnight at 4°C. Immunostaining and image processing were performed as previous described [25].

Immunoblotting

Mouse forebrains and dorsal roots were dissected, frozen on dry ice and homogenized in ice-cold homogenization buffer (0.32 M sucrose, 5 mM sodium phosphate, pH 7.2, 1 mM sodium fluoride, 1 mM sodium orthovanadate, and protease inhibitors). For dorsal roots, 10–15 roots per animal were pooled for each preparation and homogenized in 100 μl homogenization buffer. The homogenates were centrifuged at 700×*g* for 10 min at 4°C to remove nuclei and debris. For brains, the supernatant was further centrifuged at 27200×*g* for 90 min at 4°C, and the pellet was resuspended in homogenization buffer (3 ml/gram of brain). Protein concentrations were measured using a Bradford assay (Bio-Rad). The samples were resolved by SDS-PAGE, transferred to nitrocellulose membrane, and immunoblotted with the appropriate antibodies.

In vitro phosphorylation and GST-pull-down assay

GST fusion proteins were expressed in *Eschericha coli* strain BL21 (DE3) and induced by 1 mM Isopropyl β-D-1-thiogalactopyranoside (IPTG). GST fusion proteins were isolated by lysis in 0.5% Triton X-100/PBS/Complete protease inhibitor (Roche). The cells were sonicated, and proteins isolated from the cleared lysate and affinity-purified by glutathione-sepharose 4B (GE Healthcare). The protein was dialyzed against 1L 1XPBS using a 10 kD MWCO dialysis cassette (Pierce). The protein concentration was estimated from SDS gels after colloidal blue staining (Invitrogen) against a standard curve generated using bovine serum albumin, snap-frozen in liquid nitrogen, and stored at −80°C. Phosphorylation reactions were performed by incubating purified GST fusion proteins (2 ug) with 1x CKII buffer containing 200 uM ATP and 10 units of CKII (NEB, Inc) for 1 hr at 30°C. For controls, protein samples were treated identically, except CKII was omitted. *In vitro* phosphorylated GST proteins were then coated on glutathione-Sepharose 4B (GE Healthcare) by 2 hours of incubation at 4°C. At the meantime, COS7 cells transfected with full-length AnkG or AnkR were solubilized in lysis buffer [49] for 1 hour at 4°C, and then the lysates were centrifuged at 13,000×*g* for 15 min at 4°C. The soluble materials were incubated overnight with GST protein-coated beads. The beads were washed 5 times with lysis buffer and then eluted with 30 μl SDS sample buffer at 100°C for 5 min. The samples were analyzed by immunoblotting with anti-AnkG, anti-AnkR, or anti-GST antibody.

Coimmunoprecipitation

For coimmunoprecipitation, Myc-βI spectrin SR13–17 or Myc-βIV spectrin SR10–15 was co-transfected with AnkG-GFP, GFP-AnkR, or GFP in COS cells. Cells were lysed with

lysis buffer for 1 hour at 4°C and then centrifuged at 13,000×*g* for 15 min at 4°C. Protein A agarose beads (Thermo Scientific), first coated with mouse anti-GFP antibodies for 1 hour at room temperature and washed 3 times with 0.5% Triton X-100 in PBS, were then incubated with the cell lysates overnight at 4°C. After washing 5 times with lysis buffer, the beads were eluted with 20 μl of 2X reducing sample buffer at 100°C for 5 min. The samples were analyzed by immunoblot using Myc or GFP antibody. For coimmunoprecipitating NF186 and ankyrin membrane binding domains (MBD), HA-NF186 was co-transfected with Myc-AnkG MBD or Myc-AnkR MBD in HEK293 cells. The samples were immunoprecipitated with mouse anti-HA antibody and immunoblotted with Myc antibody.

Electrophysiology

Compound action potential (CAP) recording in P14 dorsal roots was performed as described [50].

Behavior analysis

P28 *Ank3*$^{F/F}$ and *Avil-Cre;Ank3*$^{F/F}$ mice were subjected to accelerating rotarod, wire hang, and hot plate tests as previously described [50].

AAV viruses and intravitreal injection

AAV2-Cre-GFP or AAV2-GFP (Vector Biolabs) was injected into the eyes of P21 *Ank3*$^{F/F}$ mice using a pulled glass needle. Both Cre and GFP were driven by their own CMV promoters. The optic nerves were dissected 2 months after virus injection, followed by immunostaining.

Reverse transcription-quantitative polymerase chain reaction (RT-qPCR)

Total RNA from the dorsal root ganglia of 1 month old mice was extracted using RNeasy Plus Mini kit (Qiagen). No DNase treatment was performed since gDNA Eliminator spin columns were used, all the primer pairs span at least one exon-exon junction and negative controls without the reverse transcriptase were included (see below). The RNA integrity was confirmed by ~2:1 intensity ratios of 28S and 18S rRNAs as sharp bands on agarose gels. cDNA was synthesized with SuperScript III First-Strand Synthesis System(Life Technologies) using random hexamers and 0.21–0.48 μg of total RNA in 20 μl of reactions. Real-time PCR was carried out using Power SYBR Green PCR master mix (Life Technologies)in 25 μl of reactions including each primer at 400 nM and 2 μl of the 4-fold diluted RT reactions on a StepOne Plus Real-Time PCR System(Life Technologies): 95°C 10 min; 40 cycles of 95°C 15 sec and 60°C 45 sec. The primers used are (5′ to 3′): AnkG (*Ank3*: forward, GTGAATGGGAACACAGCTC; reverse, TCATCGTTTCTGGGACATTC; 142-bp amplicon), AnkR (*Ank1*: forward, CCTTCGATACAGCATTCTCAG; reverse, GGAGTTAGGGTTTTCTACACG; 178-bp amplicon), βIV spectrin (*Sptbn4*: forward, GAATAAGGAGTGGCTGGAG; reverse, GATCTCACCTAATTTCTTGCG; 100-bp amplicon), βI spectrin (*Sptb*: forward, CCAAAGCCAAGCTACAAATC; reverse, CTCATTCTGCAGGGTCTG; 149-bp amplicon), and Polr2a (*Polr2a*: forward, CATCAAGAGAGTGCAGTTCG; reverse, CCATTAGTCCCCCAAGTTTG; 125-bp amplicon). The efficiency of all the primer pairs

was validated on six points of 4-fold serial dilutions of adult mouse brain cDNAs and confirmed to be between 93% and 101%. The specificity was confirmed by gel electrophoresis and sequencing from both ends of the PCR products. For all the experiments, the RT reactions without the reverse transcriptase were also carried out and included for qPCR. Either no amplification was observed or the C_q values were all higher than those derived from the RT with the reverse transcriptase by more than 5. Polr2a was chosen as the internal control in view of the previous study [51] and the tests we performed. We observed consistently close C_q values across samples in each comparison group (the SD of C_q values among different samples is 0.25–0.30). The targets were normalized to Polr2a, and all samples were then normalized to WT samples ($\Delta\Delta C_q$ method).

Statistical Analyses

Unpaired, two-tailed Student's t-test was used for statistics unless otherwise indicated. Data were collected and processed randomly and were analyzed using Microsoft Excel and GraphPad Prism. All error bars are ±SEM unless otherwise indicated. No statistical methods were used to pre-determine sample sizes, but our sample sizes are similar to those reported previously [2]. Except for electrophysiological recording, data collection and analysis were not performed blind to the conditions of the experiments. Data distribution was assumed to be normal but was not formally tested. A supplementary methods checklist is available online in the supplementary information.

Supplementary Material

Refer to Web version on PubMed Central for supplementary material.

Acknowledgments

This research was supported by NIH grants NS044916 (MNR), NS069688 (MNR), NS49119 (ECC), the Dr. Miriam and Sheldon G. Adelson Medical Research Foundation, and CURE (Citizens United for Research on Epilepsy). V.B. is an investigator of the Howard Hughes Medical Institute.

References

1. Hill AS, et al. Ion channel clustering at the axon initial segment and node of ranvier evolved sequentially in early chordates. PLoS Genet. 2008; 4:e1000317. [PubMed: 19112491]
2. Susuki K, et al. Three mechanisms assemble central nervous system nodes of Ranvier. Neuron. 2013; 78:469–482. [PubMed: 23664614]
3. Zonta B, et al. Glial and neuronal isoforms of Neurofascin have distinct roles in the assembly of nodes of Ranvier in the central nervous system. J Cell Biol. 2008; 181:1169–1177. [PubMed: 18573915]
4. Feinberg K, et al. A glial signal consisting of gliomedin and NrCAM clusters axonal Na+ channels during the formation of nodes of Ranvier. Neuron. 2010; 65:490–502. [PubMed: 20188654]
5. Thaxton C, Pillai AM, Pribisko AL, Dupree JL, Bhat MA. Nodes of Ranvier act as barriers to restrict invasion of flanking paranodal domains in myelinated axons. Neuron. 2011; 69:244–257. [PubMed: 21262464]
6. Kordeli E, Lambert S, Bennett V. AnkyrinG A new ankyrin gene with neural-specific isoforms localized at the axonal initial segment and node of Ranvier. J Biol Chem. 1995; 270:2352–2359. [PubMed: 7836469]
7. Bennett V, Baines AJ. Spectrin and ankyrin-based pathways: metazoan inventions for integrating cells into tissues. Physiol Rev. 2001; 81:1353–1392. [PubMed: 11427698]

8. Yang Y, Ogawa Y, Hedstrom KL, Rasband MN. βIV spectrin is recruited to axon initial segments and nodes of Ranvier by ankyrinG. J Cell Biol. 2007; 176:509–519. [PubMed: 17283186]
9. Gasser A, et al. An ankyrinG-binding motif is necessary and sufficient for targeting Nav1.6 Na+ channels to axon initial segments and nodes of Ranvier. J Neurosci. 2012; 32:7232–7243. [PubMed: 22623668]
10. Dzhashiashvili Y, et al. Nodes of Ranvier and axon initial segments are ankyrin G-dependent domains that assemble by distinct mechanisms. J Cell Biol. 2007; 177:857–870. [PubMed: 17548513]
11. Zhou D, et al. AnkyrinG is required for clustering of voltage-gated Na channels at axon initial segments and for normal action potential firing. J Cell Biol. 1998; 143:1295–1304. [PubMed: 9832557]
12. Pan Z, et al. A common ankyrin-G-based mechanism retains KCNQ and NaV channels at electrically active domains of the axon. J Neurosci. 2006; 26:2599–2613. [PubMed: 16525039]
13. Hedstrom KL, et al. Neurofascin assembles a specialized extracellular matrix at the axon initial segment. J Cell Biol. 2007; 178:875–886. [PubMed: 17709431]
14. Lemaillet G, Walker B, Lambert S. Identification of a conserved ankyrin-binding motif in the family of sodium channel alpha subunits. J Biol Chem. 2003; 278:27333–27339. [PubMed: 12716895]
15. Garrido JJ, et al. A targeting motif involved in sodium channel clustering at the axonal initial segment. Science. 2003; 300:2091–2094. [PubMed: 12829783]
16. Sherman DL, et al. Neurofascins are required to establish axonal domains for saltatory conduction. Neuron. 2005; 48:737–742. [PubMed: 16337912]
17. Salzer JL. Polarized domains of myelinated axons. Neuron. 2003; 40:297–318. [PubMed: 14556710]
18. Eshed-Eisenbach Y, Peles E. The making of a node: a co-production of neurons and glia. Curr Opin Neurobiol. 2013; 23:1049–1056. [PubMed: 23831261]
19. Susuki K, Rasband MN. Molecular mechanisms of node of Ranvier formation. Curr Opin Cell Biol. 2008; 20:616–623. [PubMed: 18929652]
20. Buttermore ED, Thaxton CL, Bhat MA. Organization and maintenance of molecular domains in myelinated axons. J Neurosci Res. 2013; 91:603–622. [PubMed: 23404451]
21. Zhou X, et al. Deletion of PIK3C3/Vps34 in sensory neurons causes rapid neurodegeneration by disrupting the endosomal but not the autophagic pathway. Proc Natl Acad Sci U S A. 2010; 107:9424–9429. [PubMed: 20439739]
22. Furuta Y, Lagutin O, Hogan BL, Oliver GC. Retina- and ventral forebrain-specific Cre recombinase activity in transgenic mice. Genesis. 2000; 26:130–132. [PubMed: 10686607]
23. Chan W, Kordeli E, Bennett V. 440-kD ankyrinB: structure of the major developmentally regulated domain and selective localization in unmyelinated axons. J Cell Biol. 1993; 123:1463–1473. [PubMed: 8253844]
24. Lambert S, Davis JQ, Bennett V. Morphogenesis of the node of Ranvier: co-clusters of ankyrin and ankyrin-binding integral proteins define early developmental intermediates. J Neurosci. 1997; 17:7025–7036. [PubMed: 9278538]
25. Galiano MR, et al. A distal axonal cytoskeleton forms an intra-axonal boundary that controls axon initial segment assembly. Cell. 2012; 149:1125–1139. [PubMed: 22632975]
26. Ogawa Y, et al. Spectrins and ankyrinB constitute a specialized paranodal cytoskeleton. J Neurosci. 2006; 26:5230–5239. [PubMed: 16687515]
27. Scotland P, Zhou D, Benveniste H, Bennett V. Nervous system defects of AnkyrinB (−/−) mice suggest functional overlap between the cell adhesion molecule L1 and 440-kD AnkyrinB in premyelinated axons. J Cell Biol. 1998; 143:1305–1315. [PubMed: 9832558]
28. Bennett V, Stenbuck PJ. The membrane attachment protein for spectrin is associated with band 3 in human erythrocyte membranes. Nature. 1979; 280:468–473. [PubMed: 379653]
29. Lux SE, et al. Hereditary spherocytosis associated with deletion of human erythrocyte ankyrin gene on chromosome 8. Nature. 1990; 345:736–739. [PubMed: 2141669]

30. Rasband MN, et al. Dependence of nodal sodium channel clustering on paranodal axoglial contact in the developing CNS. J Neurosci. 1999; 19:7516–7528. [PubMed: 10460258]
31. Bréchet A, et al. Protein kinase CK2 contributes to the organization of sodium channels in axonal membranes by regulating their interactions with ankyrin G. J Cell Biol. 2008; 183:1101–1114. [PubMed: 19064667]
32. Parkinson NJ, et al. Mutant beta-spectrin 4 causes auditory and motor neuropathies in quivering mice. Nat Genet. 2001; 29:61–65. [PubMed: 11528393]
33. Yang Y, Lacas-Gervais S, Morest DK, Solimena M, Rasband MN. βIV spectrins are essential for membrane stability and the molecular organization of nodes of Ranvier. J Neurosci. 2004; 24:7230–7240. [PubMed: 15317849]
34. Susuki K. Node of Ranvier disruption as a cause of neurological diseases. ASN neuro. 2013; 5:209–219. [PubMed: 23834220]
35. Leterrier C, Brachet A, Dargent B, Vacher H. Determinants of voltage-gated sodium channel clustering in neurons. Semin Cell Dev Biol. 2010; 22:171–177. [PubMed: 20934527]
36. Barry J, et al. Ankyrin-G directly binds to kinesin-1 to transport voltage-gated Na+ channels into axons. Dev Cell. 2014; 28:117–131. [PubMed: 24412576]
37. Bennett V, Healy J. Organizing the fluid membrane bilayer: diseases linked to spectrin and ankyrin. Trends Mol Med. 2008; 14:28–36. [PubMed: 18083066]
38. Zhang Y, et al. Assembly and maintenance of nodes of ranvier rely on distinct sources of proteins and targeting mechanisms. Neuron. 2012; 73:92–107. [PubMed: 22243749]
39. Chang KJ, et al. Glial ankyrins facilitate paranodal axoglial junction assembly. 2014 submitted.
40. Zhang X, Bennett V. Restriction of 480/270-kD ankyrin G to axon proximal segments requires multiple ankyrin G-specific domains. J Cell Biol. 1998; 142:1571–1581. [PubMed: 9744885]
41. Lambert S, Bennett V. Postmitotic expression of ankyrinR and beta R-spectrin in discrete neuronal populations of the rat brain. J Neurosci. 1993; 13:3725–3735. [PubMed: 8366343]
42. Kordeli E, Bennett V. Distinct ankyrin isoforms at neuron cell bodies and nodes of Ranvier resolved using erythrocyte ankyrin-deficient mice. J Cell Biol. 1991; 114:1243–1259. [PubMed: 1832678]
43. Peters LL, et al. Purkinje cell degeneration associated with erythroid ankyrin deficiency in nb/nb mice. J Cell Biol. 1991; 114:1233–1241. [PubMed: 1716634]
44. McCann SR, Jacob HS. Spinal cord disease in hereditary spherocytosis: report of two cases with a hypothesized common mechanism for neurologic and red cell abnormalities. Blood. 1976; 48:259–263. [PubMed: 949548]
45. Jenkins PM, et al. E-cadherin polarity is determined by a multifunction motif mediating lateral membrane retention through ankyrin-G and apical-lateral transcytosis through clathrin. J Biol Chem. 2013; 288:14018–14031. [PubMed: 23530049]
46. Weed SA, Stabach PR, Oyer CE, Gallagher PG, Morrow JS. The lethal hemolytic mutation in beta I sigma 2 spectrin Providence yields a null phenotype in neonatal skeletal muscle. Laboratory investigation; a journal of technical methods and pathology. 1996; 74:1117–1129.
47. Berghs S, et al. betaIV spectrin, a new spectrin localized at axon initial segments and nodes of ranvier in the central and peripheral nervous system. J Cell Biol. 2000; 151:985–1002. [PubMed: 11086001]
48. Auld VJ, et al. A rat brain Na+ channel alpha subunit with novel gating properties. Neuron. 1988; 1:449–461. [PubMed: 2856097]
49. Schafer DP, Bansal R, Hedstrom KL, Pfeiffer SE, Rasband MN. Does paranode formation and maintenance require partitioning of neurofascin 155 into lipid rafts? J Neurosci. 2004; 24:3176–3185. [PubMed: 15056697]
50. Zhang C, Susuki K, Zollinger DR, Dupree JL, Rasband MN. Membrane domain organization of myelinated axons requires betaII spectrin. J Cell Biol. 2013; 203:437–443. [PubMed: 24217619]
51. Radonić A, et al. Guideline to reference gene selection for quantitative real-time PCR. Biochem Biophys Res Commun. 2004; 313:856–862. [PubMed: 14706621]

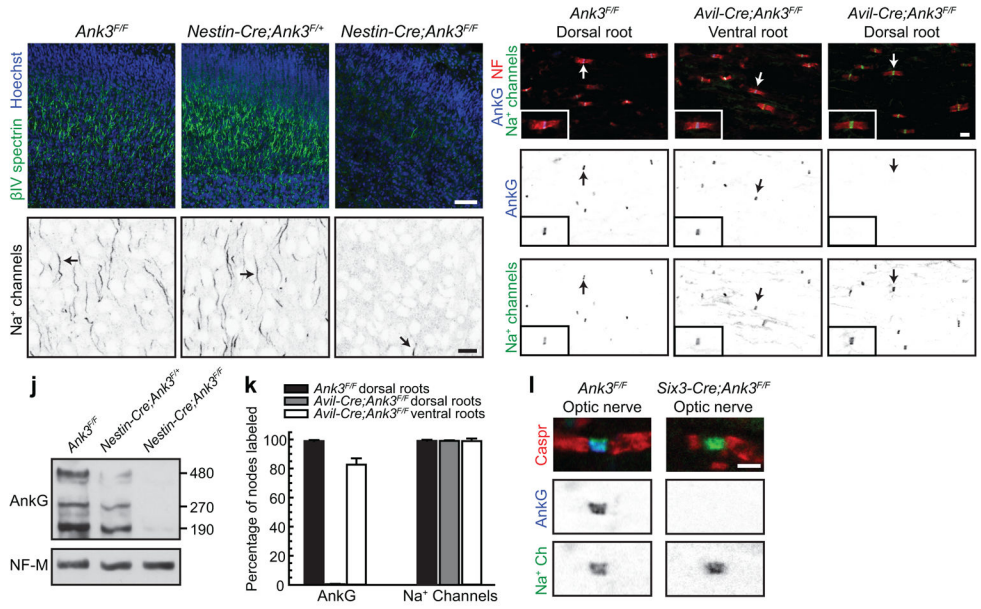

Figure 1. AnkG-deficient axons have Na+ channels clustered at nodes of Ranvier

(**a–c**) P0 *Ank3*$^{F/F}$, *Nestin-Cre; Ank3*$^{F/+}$, and *Nestin-Cre; Ank3*$^{F/F}$ mouse brain cortices stained with Hoechst to visualize nuclei (blue) and antibodies against βIV spectrin (green). Scale bar, 50 μm. (**d–f**) Axon initial segments (arrows) from P0 *Ank3*$^{F/F}$, *Nestin-Cre; Ank3*$^{F/+}$, and *Nestin-Cre; Ank3*$^{F/F}$ mouse cortices immunostained using antibodies against Na+ channels. Scale bar, 10 μm. (**g–i**) Nodes of Ranvier (arrows) from the indicated genotypes and tissues were immunostained using antibodies against neurofascin (NF, red, labels both nodal NF186 and paranodal NF155), AnkG (blue), and Na+ channels (green). Roots were collected at P14. Scale bar, 5 μm. (**j**) Immunoblot of brain homogenates from P0 *Ank3*$^{F/F}$, *Nestin-Cre; Ank3*$^{F/+}$, and *Nestin-Cre; Ank3*$^{F/F}$ mice using antibodies against AnkG. (**k**) The percentage of nodes at P14 labeled for Na+ channels and AnkG in the indicated tissues and genotypes. N= 3 animals per tissue and genotype. Error bars indicate mean +/−SEM. (**l**) Immunostaining of P30 *Ank3*$^{F/F}$ and *Six3-Cre; Ank3*$^{F/F}$ mouse optic nerves using antibodies against Caspr (red), AnkG (blue), and Na+ channels (green). Scale bar, 2 μm.

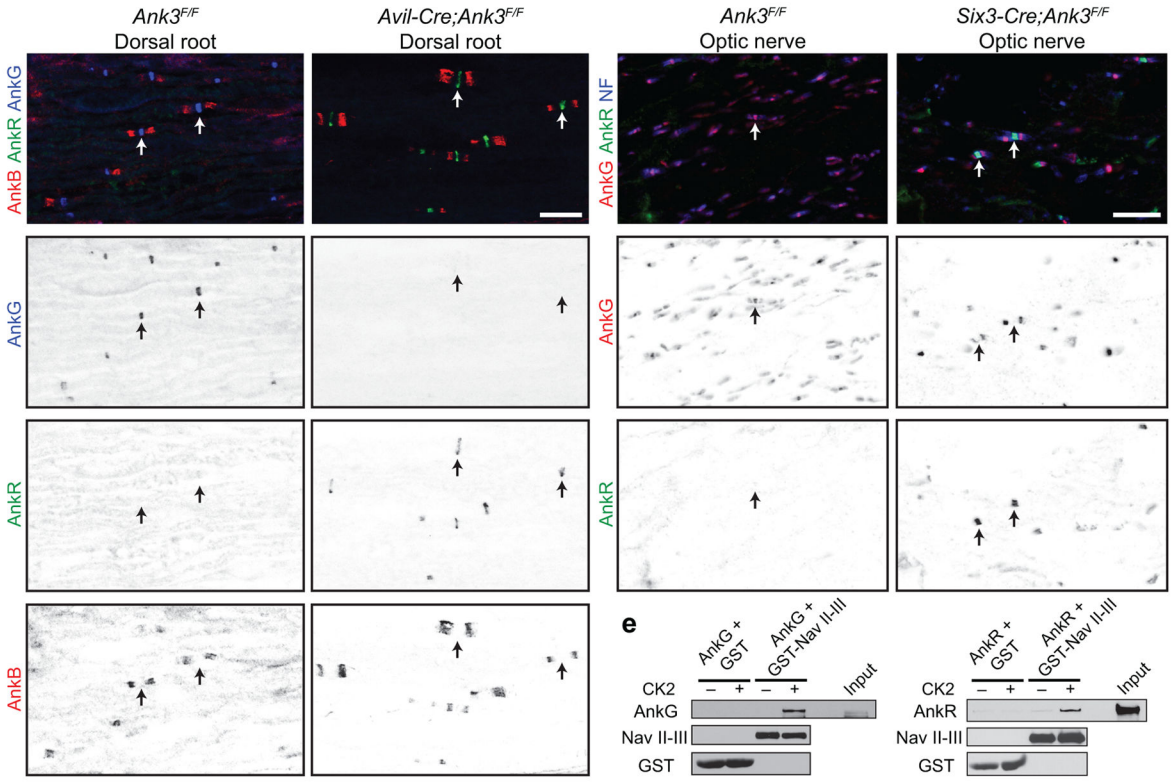

Figure 2. AnkR is found at nodes of AnkG-deficient axons and interacts with Na+ channels

(**a, b**) Immunostaining of P14 dorsal root nodes of Ranvier (arrows) from *Ank3*$^{F/F}$ and *Avil-Cre; Ank3*$^{F/F}$ mice using antibodies against AnkB (red), AnkG (blue), and AnkR (green). Scale bar, 10 μm. (**c, d**) Immunostaining of P21 optic nerve nodes of Ranvier (arrows) from *Ank3*$^{F/F}$ and *Six3-Cre; Ank3*$^{F/F}$ mice using antibodies against neurofascin (NF, blue), AnkG (red), and AnkR (green). Scale bar, 10 μm. (**e**) Pull-down assays testing the interaction between AnkG, AnkR, GST, and GST-Nav II–III. GST alone or GST-Nav II–III were incubated with CK2 to promote phosphorylation of the ankyrin-binding motif which significantly increases their affinity for ankyrins. Although both AnkG and AnkR can bind GST-Nav II–III, AnkG binds much more strongly.

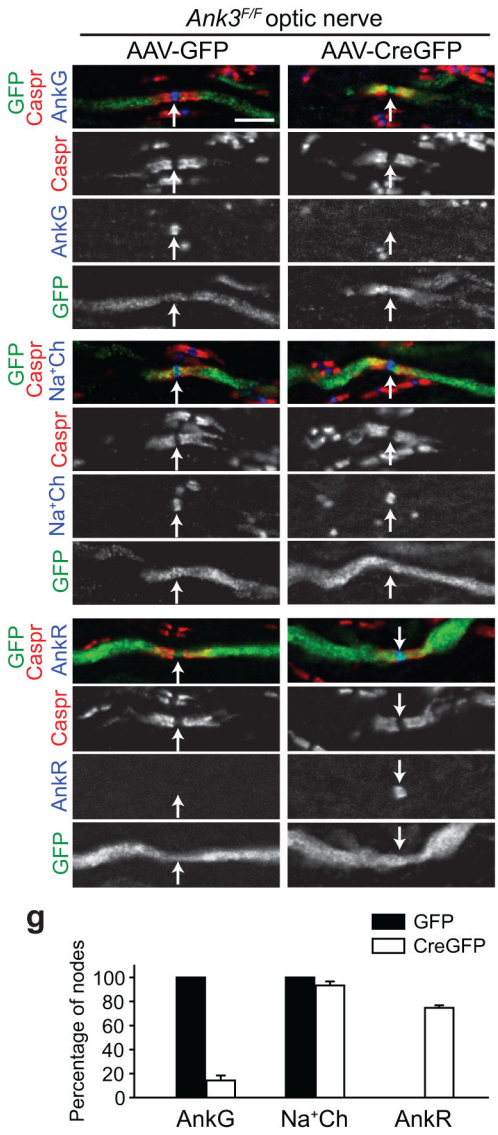

Figure 3. AnkR rescues Na+ channel clustering after loss of AnkG from adult optic nerve axons

(**a, b**) *Ank3*$^{F/F}$ mouse optic nerve nodes of Ranvier (arrows) immunostained using antibodies against Caspr (red), AnkG (blue), and GFP (green) two months after infection by AAV-GFP (**a**) or AAV-CreGFP (**b**). Scale bar, 5 μm. (**c, d**) *Ank3*$^{F/F}$ mouse optic nerve nodes of Ranvier (arrows) immunostained using antibodies against Caspr (red), Na+ channels (Na+ Ch, blue), and GFP (green) two months after infection by AAV-GFP (**c**) or AAV-CreGFP (**d**). (**e, f**) *Ank3*$^{F/F}$ mouse optic nerve nodes of Ranvier (arrows) immunostained using antibodies against Caspr (red), AnkR (blue), and GFP (green) two months after infection by AAV-GFP (**e**) or AAV-CreGFP (**f**). (**g**) Quantification of the percentage of nodes with AnkG, Na+ channels or AnkR in *Ank3*$^{F/F}$ mouse optic nerves two months after infection by AAV-GFP (N=2 optic nerves, 42 nodes were counted for AnkG; N=2, 32 nodes were counted for Na+ channels; N=2, 40 nodes were counted for AnkR) or AAV-CreGFP (N=3 optic nerves, 72 nodes were counted for AnkG; N=3, 54 nodes were

counted for Na+ channels; error bars indicate mean +/− SEM; N=2, error bar indicates the range of the data, 66 nodes were counted for AnkR).

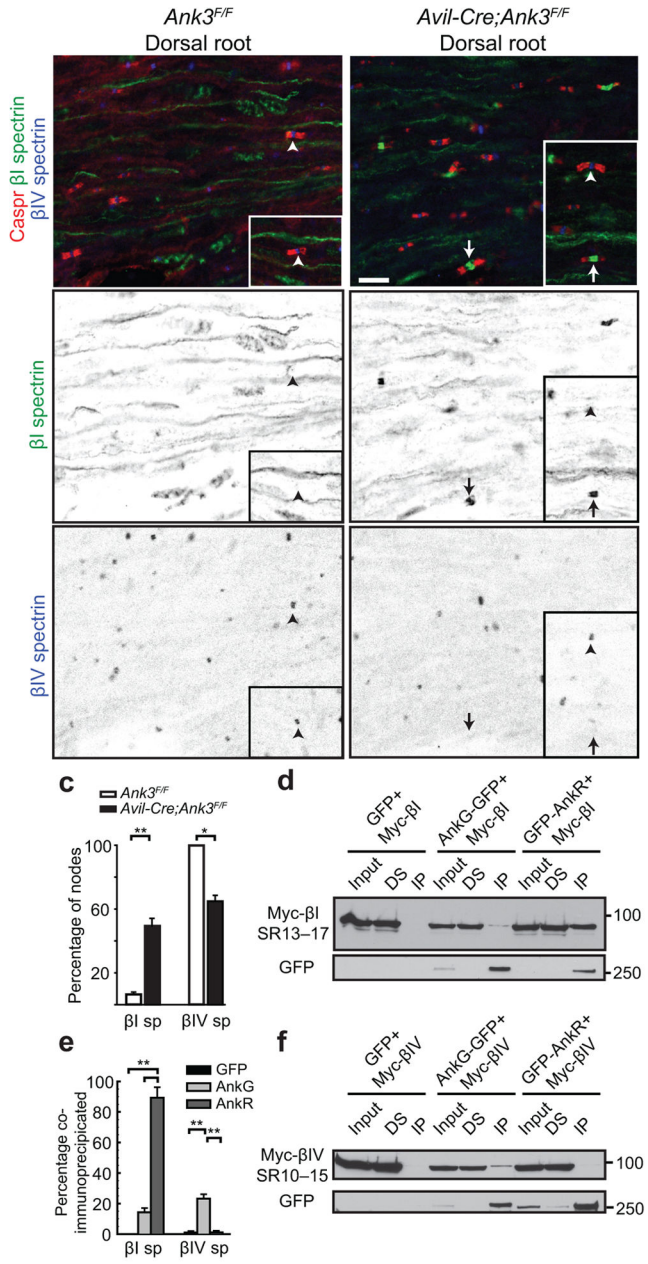

Figure 4. βI spectrin substitutes for βIV spectrin at AnkG-deficient nodes

(**a, b**) Immunostaining of P14 dorsal root nodes (arrows) from *Ank3*$^{F/F}$ (**a**)and *Avil-Cre; Ank3*$^{F/F}$ (**b**) mice using antibodies against Caspr (red), βIV spectrin (blue), and βI spectrin (green). Inset in (**b**) shows additional examples of nodes with βIV spectrin that lack βI spectrin (arrowhead) and nodes with βI spectrin that lack βIV spectrin (arrow). Scale bar, 10 μm. (**c**) Quantification of the percentage of nodes in *Ank3*$^{F/F}$ and *Avil-Cre; Ank3*$^{F/F}$ mice labeled for βIV spectrin (*p=0.011, unpaired two-tailed t-test, N=3 mice for each genotype) or βI spectrin (**p=0.007, unpaired two-tailed t-test, N=3 mice for each genotype). Error bars indicate mean +/− SEM. (**d**) Co-immunoprecipitation (IP) of AnkG-GFP or GFP-AnkR with spectrin repeats 13–17 of βI spectrin (Myc-βI SR13–17) shows βI spectrin binds

preferentially to AnkR. DS, depleted supernatant. Fusion proteins were expressed in COS cells. (**e**) Quantification of the results from co-immunoprecipitation between ankyrins and spectrins. The percent of input spectrin precipitated by the indicated GFP-fusion protein is shown. Error bars indicate mean +/−SEM. For βI spectrin co-immunoprecipitations, **p=0.0058 and 0.0035 for comparisons between AnkR and GFP, or AnkR and AnkG, respectively (two-tailed t-test, N=3 experiments). For βIV co-immunoprecipitations, **p=0.008 for comparisons between AnkG and GFP, or AnkR and AnkG (two-tailed t-test, N=3 experiments). (**f**) Co-immunoprecipitation of AnkG-GFP or GFP-AnkR with spectrin repeats 10–15 of βIV spectrin (Myc-βIV SR10–15) shows βIV spectrin binds preferentially to AnkG. Fusion proteins were expressed in COS cells.

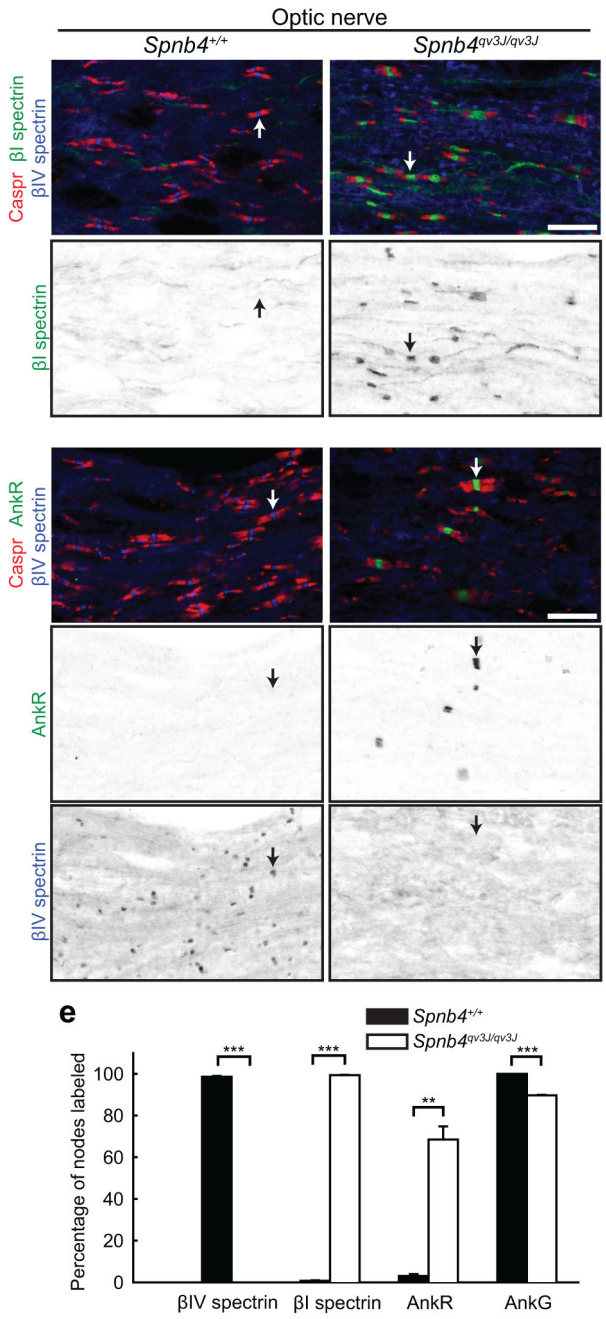

Figure 5. AnkR and βI spectrin are found at nodes of Ranvier in βIV spectrin-deficient *quivering 3J* mice

(**a, b**) Optic nerve nodes of Ranvier (arrows) from *Spnb4*$^{+/+}$(A) and *Spnb4*$^{qv3J/qv3J}$ (**b**) mice immunostained using antibodies against Caspr (red), βIV spectrin (blue), and βI spectrin (green). Scale bar, 10 μm. (**c, d**) Optic nerve nodes of Ranvier (arrows) from *Spnb4*$^{+/+}$ (**c**) and *Spnb4*$^{qv3J/qv3J}$ (**d**) mice immunostained using antibodies against Caspr (red), βIV spectrin (blue), and AnkR (green). Scale bar, 10 μm. (**e**) Quantification of the percentage of nodes in control (*Spnb4*$^{+/+}$) and *Spnb4*$^{qv3J/qv3J}$ mice labeled for βIV spectrin (***p=0.00001, unpaired two-tailed t-test, N=3 mice for each genotype), βI spectrin

(***p=0.00000016, unpaired two-tailed t-test, N=3 mice for each genotype), AnkR (**p=0.008, unpaired two-tailed t-test, N=3 mice for each genotype), or AnkG (***p=0.0001, unpaired two-tailed t-test, N=3 mice). Error bars indicate mean +/− SEM.

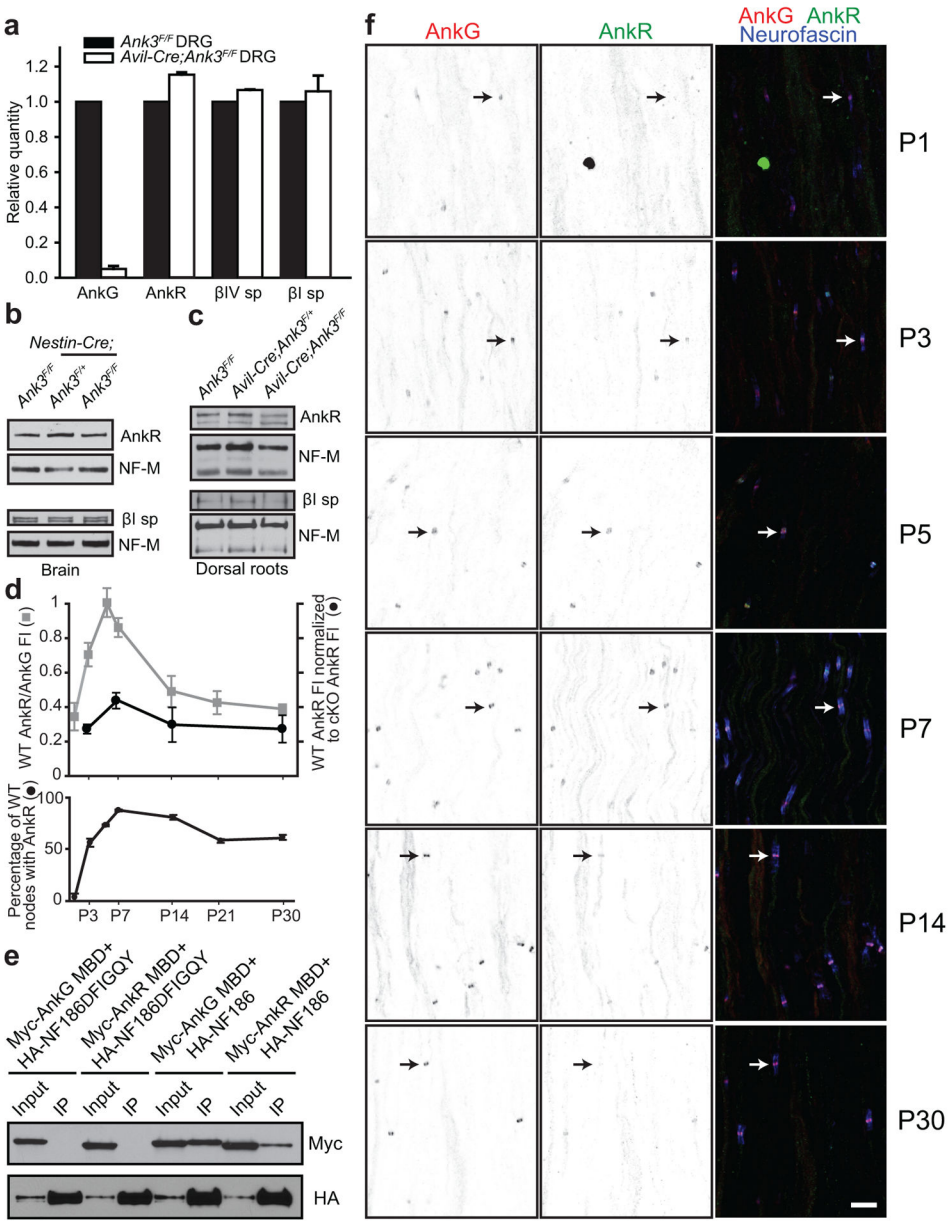

Figure 6. AnkR and βI spectrin come from a pre-existing pool of proteins

(**a**) RT-qPCR for AnkG, AnkR, βIV spectrin, and βI spectrin. RNA was collected from postnatal day 31 dorsal root ganglia of *Ank3*$^{F/F}$ and *Avil-Cre; Ank3*$^{F/F}$ mice. The targets were normalized to Polr2a, encoding RNA polymerase II polypeptide A, and all samples were then normalized to WT samples. N= 3 mice for each genotype. Error bars indicate mean +/−SEM. (**b**) Immunoblot of postnatal day 0.5 brain homogenates from *Ank3*$^{F/F}$, *Nestin-Cre; Ank3*$^{F/+}$, and *Nestin-Cre; Ank3*$^{F/F}$ mice using antibodies against AnkR, βI spectrin, and neurofilament M (NF-M). (**c**) Immunoblot of postnatal day 31 dorsal root homogenates from *Ank3*$^{F/F}$, *Avil-Cre; Ank3*$^{F/+}$, and *Avil-Cre; Ank3*$^{F/F}$ mice using antibodies against AnkR, βI spectrin, and neurofilament M (NF-M). (**d**) Quantification of the ratio of nodal AnkR fluorescence to nodal AnkG fluorescence (gray; N= 2 mice) in wild-

type mouse sciatic nerve as a function of age and the percentage of nodes with AnkR (black, lower panel; N=2 mice). Quantification of wild-type dorsal root node AnkR fluorescence intensity normalized to *Avil-Cre; Ank3*$^{F/F}$ dorsal root node AnkR fluorescence intensity (black, upper panel; N= 2 mice). Error bars indicate the range of the data. (**e**) Co-immunoprecipitation of Myc-AnkG-MBD or Myc-AnkR-MBD with HA-NF186 or HA-NF186Δ FIGQY shows NF186 preferentially binds AnkG. (**f**) Immunostaining of wild-type developing sciatic nerve from P1 to P30 using antibodies against AnkG (red) and AnkR (green). Nodes are indicated by arrows. Scale bar, 10 μm.

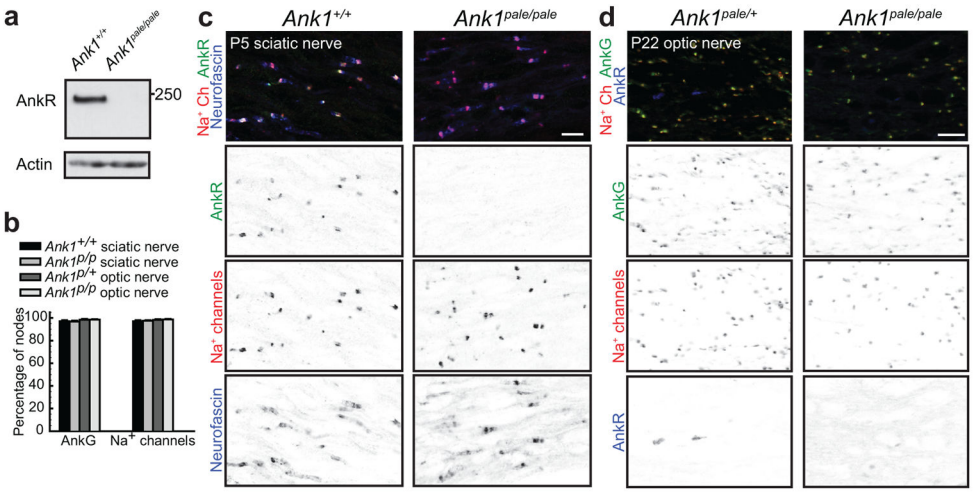

Figure 7. AnkR-deficient mice have normal PNS and CNS nodes of Ranvier

(**a**) Immunoblot of *Ank1*$^{+/+}$ *and Ank1*$^{pale/pale}$ mice using antibodies against AnkR and actin. (**b**) Quantification of the number of nodes of Ranvier labeled for AnkG or Na+ channels in control and *Ank1*$^{pale/pale}$ mice. N= 3 mice, error bars indicate mean +/− SEM. (**c**) P5 sciatic nerves from *Ank1*$^{+/+}$ *and Ank1*$^{pale/pale}$ mice immunostained using antibodies against Na+ channels (red), neurofascin (blue), and AnkR (green). Nodes formed normally in both genotypes. Scale bar, 10 μm. (**d**) P22 optic nerves from *Ank1*$^{pale/+}$ *and Ank1*$^{pale/pale}$ mice immunostained using antibodies against Na+ channels (red), AnkR (blue), and AnkG (green). Nodes formed normally in both genotypes. Scale bar, 10 μm.

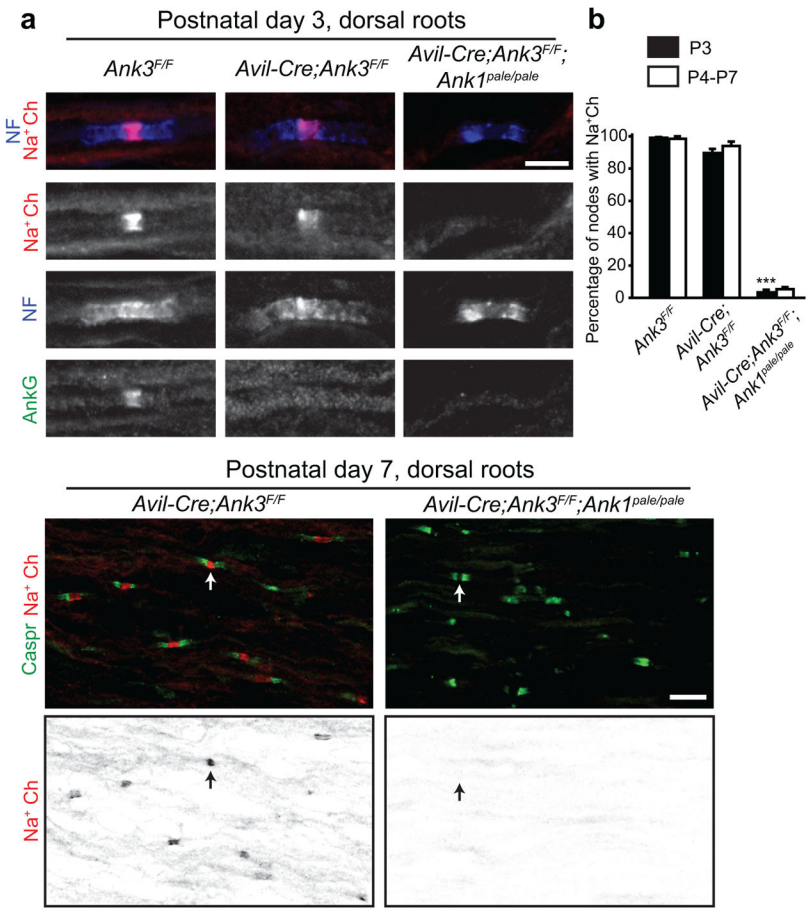

Figure 8. Ankyrins are required for Na+ channel clustering at nodes of Ranvier

(**a**) Immunostaining of P3 dorsal root nodes of Ranvier from *Ank3*$^{F/F}$, *Avil-Cre; Ank3*$^{F/F}$, and *Avil-Cre; Ank3*$^{F/F}$*;Ank1*$^{pale/pale}$ using antibodies against Na+ channels (red), neurofascin (NF, blue), and AnkG (green). Scale bar, 5 μm. (**b**) Quantification of the percentage of nodes of Ranvier with Na+ channels in *Ank3*$^{F/F}$, *Avil-Cre; Ank3*$^{F/F}$, and *Avil-Cre; Ank3*$^{F/F}$*;Ank1*$^{pale/pale}$ mice at P3 and P4–P7. *Ank3*$^{F/F}$ vs. *Avil-Cre; Ank3*$^{F/F}$*;Ank1*$^{pale/pale}$ (***p=0.0001, unpaired two-tailed t-test, N= 3 mice for each genotype at P3). *Avil-Cre; Ank3*$^{F/F}$ vs. *Avil-Cre; Ank3*$^{F/F}$*;Ank1*$^{pale/pale}$ (***p=0.00003, unpaired two-tailed t-test, N=3 mice for each genotype at P3). Error bars indicate mean +/−SEM. For the P4–P7 time point, the number of nodes were pooled from one animal at P4 and one at P7 for each genotype. Error bars indicate the range of the data. (**c, d**) Immunostaining of P7 sciatic nerve nodes of Ranvier from *Avil-Cre; Ank3*$^{F/F}$ (**c**) and *Avil-Cre; Ank3*$^{F/F}$*;Ank1*$^{pale/pale}$ (**d**) using antibodies against Na+ channels (red) and Caspr (green). Scale bar, 10 μm.